Article

Structure

Negative Regulation of Peptidyl-Prolyl Isomerase Activity by Interdomain Contact in Human Pin1

Graphical Abstract

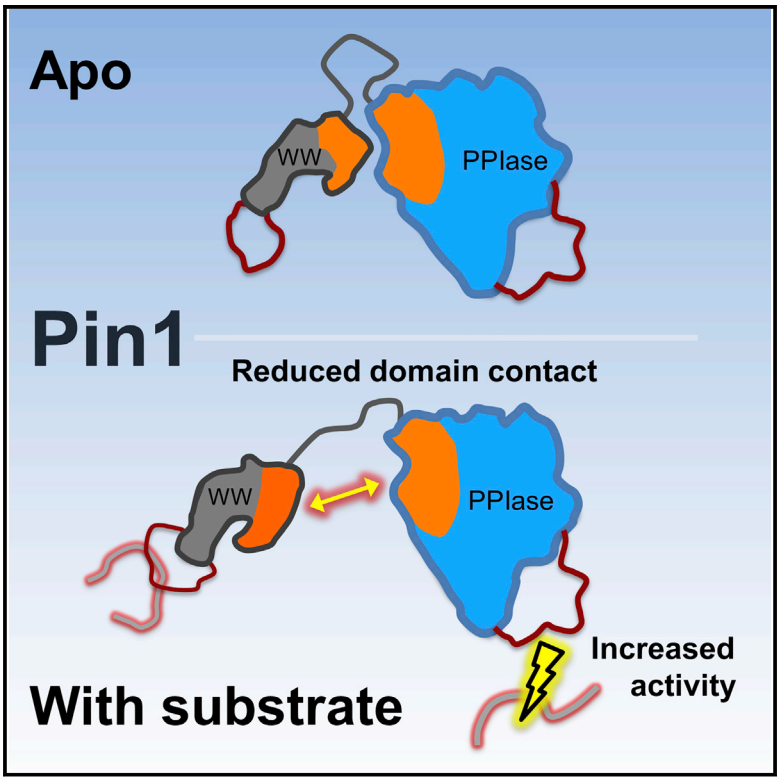

Authors

Xingsheng Wang, Brendan J. Mahoney, Meiling Zhang, John S. Zintsmaster, Jeffrey W. Peng

Correspondence

jpeng@nd.edu

In Brief

Pin1 is a two-domain cell cycle enzyme that catalyzes the *cis-trans* isomerization of phospho-S/T-P motifs. Wang et al. use NMR to examine Pin1 mutants and reveal a phosphopeptide substrate that reduces interdomain contact while enhancing isomerase activity; this suggests negative allosteric regulation of the catalytic site by interdomain contact.

Highlights

- Investigated interplay between interdomain contact and activity in Pin1
- Studied Pin1 mutants that perturb interdomain contacts or substrate interaction
- Reduced interdomain contact yields enhanced isomerase activity
- Results suggest interdomain contact can allosterically regulate Pin1 activity

Wang et al., 2015, Structure *23*, 2224–2233
December 1, 2015
http://dx.doi.org/10.1016/j.str.2015.08.019

CellPress

Structure
Article

Negative Regulation of Peptidyl-Prolyl Isomerase Activity by Interdomain Contact in Human Pin1

Xingsheng Wang,[1] Brendan J. Mahoney,[1] Meiling Zhang,[1] John S. Zintsmaster,[1] and Jeffrey W. Peng[1,*]
[1]Department of Chemistry and Biochemistry, University of Notre Dame, 251 Nieuwland Science Hall, Notre Dame, IN 46556, USA
*Correspondence: jpeng@nd.edu
http://dx.doi.org/10.1016/j.str.2015.08.019

SUMMARY

Pin1 is a modular peptidyl-prolyl isomerase specific for phosphorylated Ser/Thr-Pro (pS/T-P) motifs, typically within intrinsically disordered regions of signaling proteins. Pin1 consists of two flexibly linked domains: an N-terminal WW domain for substrate binding and a larger C-terminal peptidyl-prolyl isomerase (PPIase) domain. Previous studies showed that binding of phosphopeptide substrates to Pin1 could alter Pin1 interdomain contact, strengthening or weakening it depending on the substrate sequence. Thus, substrate-induced changes in interdomain contact may act as a trigger within the Pin1 mechanism. Here, we investigate this possibility via nuclear magnetic resonance studies of several Pin1 mutants. Our findings provide new mechanistic insights for those substrates that reduce interdomain contact. Specifically, the reduced interdomain contact can allosterically enhance PPIase activity relative to that when the contact is sustained. These findings suggest Pin1 interdomain contact can negatively regulate its activity.

INTRODUCTION

Human Pin1 is a peptidyl-prolyl isomerase that mediates numerous protein-protein interactions regulating cell growth. It targets phospho-Ser/Thr-Pro (pS/TP) motifs in mobile or intrinsically disordered regions (IDRs) of other signaling proteins (Lee et al., 2014), to catalyze the *cis-trans* isomerization of the imide linkage between pS/T and P (Lu et al., 1996; Yaffe et al., 1997). Pin1 substrates include mitotic regulators (Lu and Zhou, 2007) relevant for oncogenesis, such as Cdc25C phosphatase (Crenshaw et al., 1998), c-Myc (Yeh et al., 2004), and p53 (Wulf et al., 2002), and neuronal proteins relevant for Alzheimer's disease, such as Tau (Lu et al., 1999) and the amyloid precursor protein (Pastorino et al., 2006).

Pin1 is modular, consisting of two flexibly linked domains: a non-catalytic N-terminal WW domain (residues 1–39) for substrate binding, and a catalytic C-terminal domain (residues 50–163) with peptidyl-prolyl isomerase (PPIase) activity (Figures 1A and 1B). Both domains specifically bind pS/T-P motifs. Previous studies have pointed to cross-talk between the two domains. For example, WW domain binding to a non-isomerizable pT-P motif decreases PPIase activity at a distinct pS/T-PpSL site in tau peptides (Smet et al., 2005). Point mutations (Poolman et al., 2013; Sami et al., 2011) and post-translational modifications (Chen et al., 2013; Lee et al., 2011; Lu et al., 2002) in the WW domain alter PPIase activity and Pin1 subcellular location.

Nevertheless, the mechanism for Pin1 interdomain cross-talk has remained murky. An appealing possibility is the set of interdomain contacts revealed by Pin1 X-ray crystal structures (Ranganathan et al., 1997; Verdecia et al., 2000). Nuclear magnetic resonance (NMR) showed that these contacts are transient (Bayer et al., 2003; Jacobs et al., 2003), weakening or strengthening upon binding of phosphopeptide substrates (Jacobs et al., 2003). Thus, dynamic interdomain contact may somehow facilitate cross-talk.

Recently we described a Pin1 mutant, I28A, which decreased interdomain contact in apo Pin1, yet increased PPIase isomerase activity (Wilson et al., 2013). While we were tempted to interpret this as negative regulation of PPIase activity by interdomain contact, we balked because I28A also weakened the substrate-binding affinity to the WW domain. For stronger conclusions, we needed to perturb substrate binding without direct perturbation at the interdomain interface.

Here, we describe investigations meeting this need. In particular, we have generated new Pin1 mutants that separately perturb catalysis and substrate binding, and have characterized their interactions with a phosphopeptide substrate we have used in previous studies of Pin1 functional dynamics (Namanja et al., 2007; Wilson et al., 2013). The phosphopeptide, EQPLpTPVTDL, corresponds to a Pin1 target site (pT48-P49) within the N-terminal disordered region of Cdc25C, and mitotic phosphatase and Pin1 substrate (Zhou et al., 2000). Henceforth, we refer to EQPLpTPVTDL as pCdc25C.

Our new findings indicate that pCdc25C binding to the WW domain perturbs distal WW residues mediating transient contact with the PPIase domain. The perturbations reduce interdomain contact, thereby enhancing both interdomain mobility and *cis-trans* isomerase activity at the distal PPIase catalytic site. Thus, we propose that interdomain contact within Pin1 can provide negative allosteric regulation of the PPIase catalytic site.

RESULTS

Rationale for Pin1 Mutants

We investigated Pin1 variants containing Ala substitution mutations R68A-Pin1, R68A/R69A-Pin1, W34A-Pin1, and I28A-Pin1 (Figure 1A). Earlier enzymatic (Yaffe et al., 1997) and fluorescence binding studies (Verdecia et al., 2000) identified these

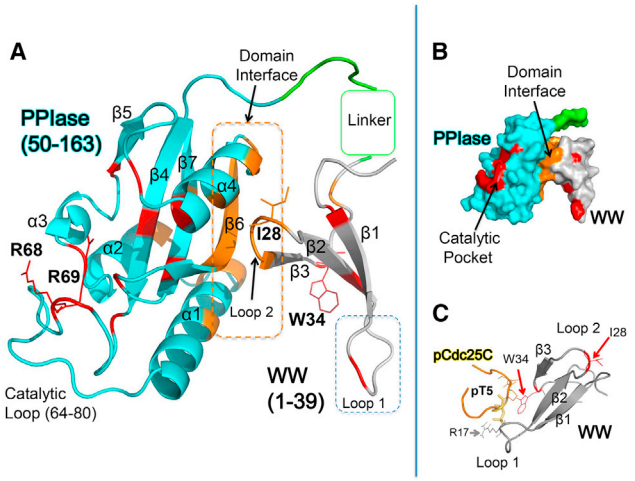

Figure 1. Structural Features of Pin1

(A) Ribbon representation of Pin1 modular organization (PDB: 1PIN) (Ranganathan et al., 1997): N-terminal WW domain (gray), flexible linker (green), and a C-terminal PPIase domain (cyan). Functional loops are annotated. Additional shading: residues contacting substrate (red); interdomain interface residues (orange). Sites of alanine substitutions (bold font and side-chain lines) include R68/R69 (left), I28 (middle), and W34 (right).

(B) 1PIN surface rendering, following the color scheme of (A).

(C) Binding interactions between substrate pCdc25C (EQPLpTPVTDL) and the Pin1 WW domain (PDB: 1I8G) (Wintjens et al., 2001). W34 and Loop 1 (S16-R21) make principal contacts with pCd25C. Loop 2 (H27-N30), which includes I28, makes transient contacts with the PPIase domain.

mutants as having consequences appropriate for separate perturbation of isomerase activity, substrate binding by the WW domain, and interdomain contact. For example, R68A-Pin1 and R68A/R69A-Pin1 selectively perturbed *cis-trans* isomerization. R68 and R69 are in the PPIase flexible loop (H64-R80) capping the PPIase active site (Figure 1A). Their basic side chains make key contacts with the substrate pS/T moiety; previous enzyme assays showed that R68A/R69A substitutions reduced isomerase activity by >500-fold (Yaffe et al., 1997). W34A-Pin1 perturbed substrate binding by removing polar interactions between the W34-εNH side chain and the substrate pS/T moiety (Verdecia et al., 2000; Wintjens et al., 2001). Early fluorescence anisotropy showed that W34A reduced WW domain binding affinity by ~30-fold (Verdecia et al., 2000). Critically, W34A avoids direct perturbation of interdomain interface residues, such as loop 2 (H27-N30) (Figure 1C). Finally, both I28A-Pin1 and the isolated PPIase domain perturbed the interdomain interface (orange shading in Figures 1A and 1B). Critically, I28 lacks direct contact with substrate or W34 (Figure 1C); it resides in loop 2, which mediates contact with the PPIase domain. I28A weakens WW-PPIase domain contact (Wilson et al., 2013). The isolated PPIase domain entailed deleting WW residues 1–39; this construct emulated complete removal of interdomain contact.

Activity of Pin1 Mutants

We recorded 2D ^{15}N-^{1}H heteronuclear single-quantum coherence (HSQC) NMR spectra of the above constructs (Figure S1); the number and dispersion of NH cross-peaks indicated preservation of the overall fold.

Table 1. *cis-trans* Isomerase Activity (k_{EXSY}) and K_D Values for Pin1 Variants

Variant	k_{TC} (s^{-1})	k_{CT} (s^{-1})	k_{EXSY} (s^{-1})	K_D (μM)	Interdomain Contact[a]
WT-Pin1	31.3 (1.0)	2.00 (0.06)	33.3 (1.1)	9 (1)	–
R68A/R69A	–[b]	–	–	11 (1)	=WT
W34A	17.2 (0.3)	0.98 (0.01)	18.2 (0.4)	>2000[c]	>WT
I28A	71.0 (1.0)	2.43 (0.04)	73.0 (2.0)	55 (5)	<WT
Isolated PPIase	39.4 (1.0)	2.00 (0.04)	41.0 (0.4)	NA[d]	None

Measurements at 295 K, pH 6.6, 16.4 T. Rate constants $k_{EXSY} = k_{TC} + k_{CT}$ recorded on 2 mM pCdc25C, 50 μM protein. Uncertainty estimates are in parentheses.

[a]Interdomain contact relative to apo WT-Pin1, based on NH CSPs of Figures 2 and 3.

[b]Measurements were for R68A-Pin1; negligible isomerase activity.

[c]W34A-Pin1 ^{15}N-^{1}H CSPs indicated <50% binding saturation after adding 2.2 mM pCdc25C to 50 μM protein.

[d]NMR titration data unavailable; initial isothermal titration calorimetry measurements of isolated PPIase domain indicate K_D > 1 mM.

We compared the isomerase activities of the Pin1 constructs by collecting 2D ^{1}H-^{1}H exchange spectra (Jeener et al., 1979) of pCdc25C. For each Pin1 construct, we determined the net exchange rate constant, k_{EXSY}, for *cis-trans* isomerization of the pT methyl protons of pCdc25C. We also estimated the equilibrium dissociation constants, K_D (binding affinities), between pCdc25C and the Pin1 constructs by titrating in pCdc25C, and following the protein backbone ^{15}N-^{1}H chemical shift perturbations (CSPs), defined in Equation 1 in Experimental Procedures. The k_{EXSY} and K_D values are summarized in Table 1.

Backbone Chemical Shift Perturbations Related to Mutations and Binding

To understand the effects of the mutations, we examined their backbone ^{15}N-^{1}H CSPs (Figure 2). The CSPs for the isolated PPIase domain (panel i) were of particular interest because they reflected the elimination of interdomain contact. Beyond the expected edge effect (e.g. N terminus), the most significant CSP segment was the surge at the α4/β6 region (e.g. F139, A140, L141, R142, S147). These CSPs localized to interdomain interface residues in the 1PIN crystal structure (Figures 1A and 1B) (Ranganathan et al., 1997), and were consistent with CSPs from a slightly different lone PPIase construct (Bayer et al., 2003). Accordingly, we treated the α4/β6 CSP surge as an indicator of reduced interdomain contact, and used it to interpret other CSP profiles. Among the apo full-length variants, only I28A-Pin1 (Figure 2, panel iv) reproduced the α4/β6 CSP surge, indicating reduced interdomain contact relative to wild-type Pin1 (WT-Pin1). By contrast, W34A and R68A/R69A caused only minimal perturbations to interdomain contact. Notably, the most significant CSPs of R68A/R69A were at catalytic residues.

The α4/β6 CSP surge also helped clarify the effects of adding saturating amounts of pCdc25C substrate (Figure 3A). In particular, adding pCdc25C to WT-Pin1 reproduced the α4/β6 CSP surge, indicating that pCdc25C binding decreased interdomain contact. By contrast, adding pCdc25C to W34A-Pin1 and I28A-Pin1 failed to reproduce the α4/β6 CSP surge. Thus,

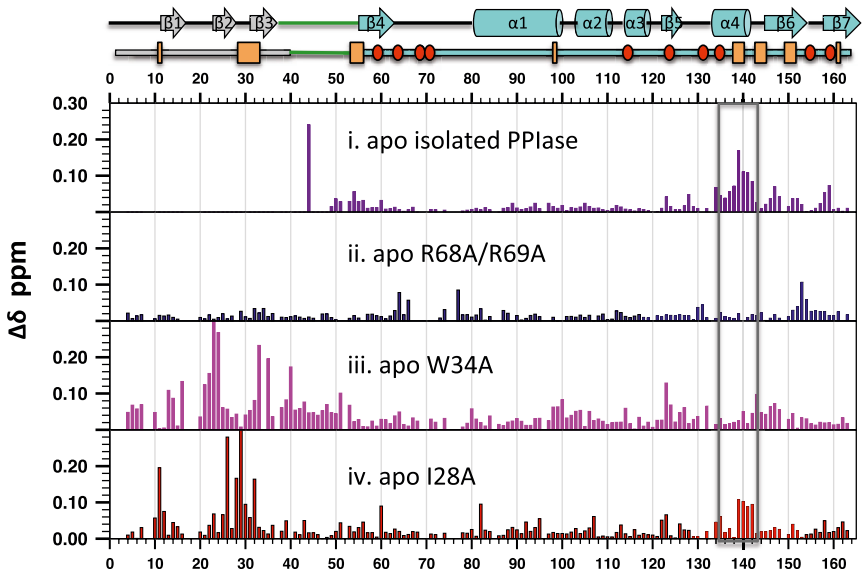

Figure 2. CSPs to apo Protein from Mutations

Backbone NH chemical shift perturbations (CSPs) of apo WT-Pin1 caused by (i) WW domain deletion, (ii) R68A/R69A, (iii) W34A, and (iv) I28A. Secondary structure elements are indicated in the banner above. The banner highlights catalytic pocket residues (red ovals) and interdomain interface residues (orange rectangles).

W34A- and I28A-Pin1 retained their apo levels of interdomain contact, but for different reasons. For W34A-Pin1, the W34A substitution essentially eliminated pCdc25C binding to its WW domain (K_D >2 mM, Table 1). Therefore, its lack of a α4/β6 CSP surge reflected insufficient pCdc25C binding to the WW domain, the key event triggering the loss of interdomain contact. For I28A-Pin1, its apo state interdomain contact was *already* reduced relative to apo WT-Pin1, because of the I28A substitution (Figure 2, panel iv). In effect, apo I28A-Pin1 lacked any significant interdomain contact for substrate binding to perturb; hence, the addition of pCdc25C failed to reproduce the CSP surge. The R68A/R69A substitutions destroyed isomerase activity without perturbing WW domain substrate binding or interdomain contact. Hence, R68A/R69A-Pin1 retained the WT α4/β6 CSP surge, indicating reduced interdomain contact. Its main differences from WT-Pin1 were the lack of CSPs at catalytic residues.

The CSP directions for residues 134–142 gave another spectral phenotype for reduced interdomain contact. Examples are A140 and L141 cross-peaks in Figure 3B. These residues are at the α4/β6 juncture; they gave a distinct upfield shift in the isolated WT-PPIase domain (purple) compared with full-length WT-Pin1 (black), and served as additional diagnostics of reduced contact. Inspection of the other A140-L141 cross-peaks indicated that I28A (red) and pCdc25C-bound WT-Pin1 (green) both caused a significant loss of interdomain contact, whereas W34A (magenta) and R68A/R69A did not (cross-peaks not shown because they were coincident with WT).

Insights from Heteronuclear Spin Relaxation

In parallel, we have been investigating the functional motions of Pin1 side chains on the microsecond-to-millisecond timescale. Our first study of Pin1 side-chain dynamics included $^{13}C_{methyl}$ R_2 measurements on 50% perdeuterated, uniformly ^{13}C-labeled Pin1 (Namanja et al., 2007). The uniform ^{13}C labeling called for constant time periods to minimize ^{13}C-$^{13}C_{methyl}$ J-coupling artifacts, decreasing spectral sensitivity. Here, we generated ILV-labeled (U-^{15}N, Ileδ-[$^{13}CHD_2$]-, Leuδ_1/δ_2-[$^{13}CHD_2$]$_2$-, and Valγ_1/γ_2-[$^{13}CHD_2$]$_2$-), which put ^{12}C next to $^{13}C_{methyl}$, thereby removing ^{13}C-$^{13}C_{methyl}$ J-coupling concerns (Tugarinov and Kay, 2004). Accordingly, the ILV samples enabled more precise $^{13}C_{methyl}$ R_2 measurements (for example spectra see Figure S2). Serendipitously, these R_2 further illuminated the effects of pCdc25C binding on interdomain contact (see below).

Figure 4A shows $\Delta R_2 = R_{2,pCdc25C} - R_{2,APO}$, the change in $^{13}C_{methyl}$ R_2 upon addition of a 7-fold excess of pCdc25C. The R_2 measurements used Carr-Purcell-Meiboom-Gill (CPMG) interpulse delays of 900 μs, with values given in Figure S3A, where the WT-Pin1 $^{13}C_{methyl}$ R_2 changes are in the top bar graph; its methyl sites are the spheres in Figure 4B. While I78δ in the PPIase catalytic loop showed a large increase ($R_{2,pCdc25C} > R_{2,APO}$), all other methyls showed decreases ($R_{2,pCdc25C} < R_{2,APO}$), ranging from 4% to 48% relative to the apo state ($R_{2,pCdc25C} < R_{2,APO}$). The trimmed average decrease was -0.9 s^{-1}. Conspicuously large decreases occurred for L7$\delta_{1,2}$ and interdomain interface methyls, including V22δ_2 and I28δ in the WW domain, and L141δ_2 and V150γ_2 in the PPIase domain α4/β6. These methyls correspond to the deep-blue spheres in Figure 4B; notably, they coincided with methyls showing the largest $^{13}C_{methyl}$ CSPs (Figure S2C).

In Figure 4A, the lower panel shows changes for both W34A-Pin1 (filled green bars) and I28A-Pin1 (open violet bars). W34A-Pin1 $^{13}C_{methyl}$ R_2 values were unchanged upon addition of pCdc25C, within the estimated uncertainties. The I28A-Pin1 $^{13}C_{methyl}$ R_2 values decreased significantly for L7$\delta_{1,2}$, but elsewhere, particularly at the interdomain interface, they remained unchanged. Thus, W34A-Pin1 and I28A-Pin1 failed to reproduce the WT-Pin1 pCdc25C-induced relaxation response, just as they failed to reproduce the WT-Pin1 pCdc25C-induced α4/β6 CSP surge (Figure 3, panels iii and iv versus i). As stated, the WT α4/β6 CSP surge (Figure 3, panel i) indicates a loss of interdomain contact upon pCdc25C binding. This does not occur for W34A-Pin1 and I28A-Pin1, either because of a severe loss of pCdc25C-binding affinity (W34A-Pin1), or a severe loss of interdomain contact prior to pCdc25C addition (I28A-Pin1). These facts suggest that the pCdc25C-induced decreases in $^{13}C_{methyl}$ R_2 for WT-Pin1 (Figure 4A, top) also reflected reduced interdomain contact, triggered by pCdc25C binding to the WW domain.

To explain how pCdc25C binding could decrease the WT-Pin1 $^{13}C_{methyl}$ R_2 values, we considered quenching of microsecond-millisecond exchange dynamics in apo WT-Pin1, or changes in the reorientational nanosecond mobility of the $^{13}C_{methyl}$-$^{1}H_{methyl}$

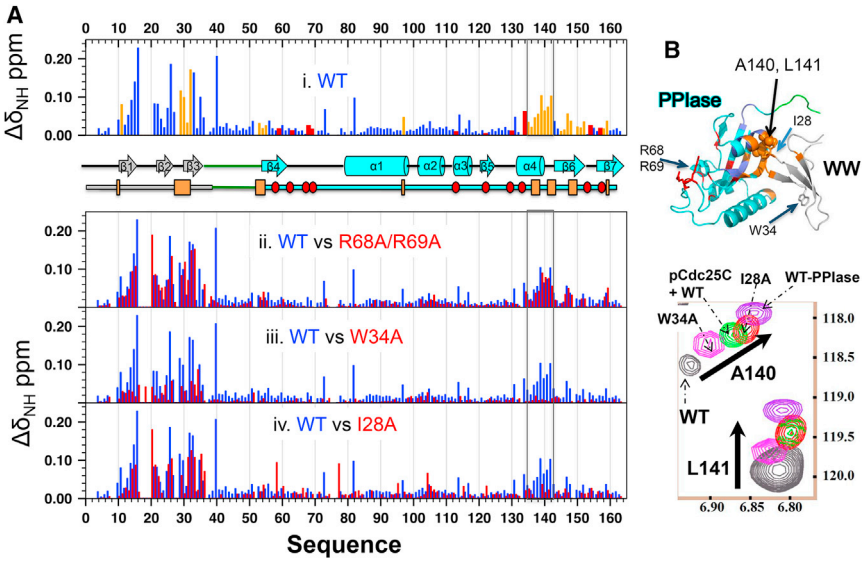

Figure 3. Backbone NH Chemical-Shift Perturbations due to pCdc25 Binding

(A) Top: (i) pCdc25C-induced chemical-shift perturbations (CSPs) of WT-Pin1 from previous work (Namanja et al., 2007). Default shading of WT bars is blue. Red and orange bars indicate catalytic pocket and interdomain interface residues, respectively. The banner below indicates secondary structure, and residues in the catalytic pocket (red ovals) and domain interface (orange rectangles). Bar graphs under the banner overlay pCdc25C-indcued CSPs of WT (blue) with the variants (red), and include (ii) R68A/R69A, (iii) W34A, and (iv) I28A from Wilson et al. (2013). Only R68A/R69A shows the CSP surge at the interdomain interface (α4/β6) characteristic of pCdc25C binding to WT-Pin1.

(B) A140 and L141, at the interdomain interface region (orange) of the PPIase domain (α4/β6) indicated on 1PIN (Ranganathan et al., 1997). Their NH cross-peak positions (chemical shifts) are diagnostic of the degree of interdomain contact. Cross-peak color coding is: black, apo WT-Pin1; magenta, apo W34A-Pin1; green, pCdc25C-WT-Pin1; red, apo I28A-Pin1; purple, apo isolated PPIase domain.

bonds. To explore the possibility of exchange dynamics, we followed our previous study (Namanja et al., 2007) and identified the high outliers in the product $^{13}C_{methyl}$ R_1*R_2 as $^{13}C_{methyl}$ nuclei experiencing microsecond-millisecond exchange dynamics (Kneller et al., 2002). The outliers agreed with those of our previous study (Namanja et al., 2007), and included the methyls with large pCdc25C-induced decreases in R_2 as per Figures 4A and 4B. Accordingly, we took these methyls as having $^{13}C_{methyl}$ R_2 values with exchange contributions, R_{ex}, sensitive to reduced interdomain contact caused by pCdc25C binding. The $^{13}C_{methyl}$ R1*R_2 values for the WT-Pin1 ILV methyls, and their comparison with our previous estimates (Namanja et al., 2007), are shown in Figure S3B.

To characterize the exchange dynamics giving rise to these R_{ex} contributions, we measured $^{13}C_{methyl}$ CPMG relaxation dispersion profiles (Loria et al., 1999; Skrynnikov et al., 2001), $R_{2,eff}$ versus ν_{CPMG}, for the apo and pCdc25C-saturated states of WT-Pin1, I28A-Pin1, and W34A-Pin1. The CPMG spin-lock frequency varied from 93 s^{-1} < ν_{CPMG} < 500 s^{-1}. Except for I78δ and V62γ1, we observed flat $R_{2,eff}$ profiles, i.e. no dispersion (Figure S4). The flatness indicated exchange rate constants exceeding our maximum CPMG spin-lock frequency ~2π*500 s^{-1}. Quantitative estimates of the exchange rates will require higher spin-lock strengths, such as those in off-resonance $R_{1\rho}$ measurements (Mulder et al., 1998). We also note that an effective way to quantify the exchange-free portion of R_2, and thus resolve R_{ex}, is measurement of transverse cross-correlated relaxation as reported by Kay and co-workers (Tugarinov et al., 2004).

We had previously identified these ^{13}C methyls (i.e. L7δ_1, L7δ_2, V22γ_2, I28δ, L141δ_2, and V150γ_2) as exchange-sensitive sites (Namanja et al., 2007); however, the nature of the underlying exchange dynamics was murky. The present work provides new insight: the exchange dynamics are likely related to the transient interdomain contact within apo Pin1. The decreased exchange upon pCdc25C binding to the WW domain likely reflects the stabilization of more extended interdomain dispositions (loss of interdomain contact).

While exchange dynamics accounted for the largest-magnitude $^{13}C_{methyl}$ R_2 decreases, the nearly uniform background reduction of ~0.9 s^{-1} still required an explanation (Figure 4A, open blue bars). The uniformity focused us on the overall reorientational mobility of the two domains. Using a reduced spectral density mapping procedure (Peng and Wagner, 1995), we converted WT-Pin1 ^{15}N R_1, R_2, and steady-state nuclear Overhauser effect (ssNOE) values to $J_{eff}(0)$ values. This procedure makes no a priori assumptions about the NH bond motions, other than a flat power spectral density function in the high frequency region $\omega_H \pm \omega_N$, reasonable for proteins studied at high B_0 (Peng and Wagner, 1995). Physically, $J_{eff}(0)$ represents an effective correlation time for each NH bond (Peng and Wagner, 1992); it becomes the same for all NH bonds if the protein is a rigid, isotropically tumbling molecule. We plotted $J_{eff}(0)$ for apo WT-Pin1 (horizontal axis) versus $J_{eff}(0)$ for pCdc25C-saturated WT-Pin1 (vertical axis) in Figure 4C. If pCdc25C binding changed the WW and PPIase domain motions in the same way, then all points should fall on one line. Instead, the WW and PPIase domain NH bonds produced *distinct* slopes (WW slope = 0.68, correlation coefficient of 0.94; PPIase slope = 0.84, correlation coefficient of 0.9), indicating that pCdc25C induced a differential increase in domain mobility, consistent with reduced contact between domains of different size.

In summary, our heteronuclear relaxation studies indicated two independent causes for the WT-Pin1 decrease in $^{13}C_{methyl}$ R_2 in Figure 4A: (1) enhanced nanosecond rotational mobility of the WW domain relative to the PPIase domain; and (2) quenching of microsecond exchange dynamics unique to the apo state, which are likely related to interdomain mobility responsible for the transient interdomain contacts of apo Pin1.

DISCUSSION

In Pin1, peptidyl-prolyl isomerization occurs solely within the PPIase domain. Our results indicate that pCdc25C binding to the WW domain triggers a decrease in interdomain contact,

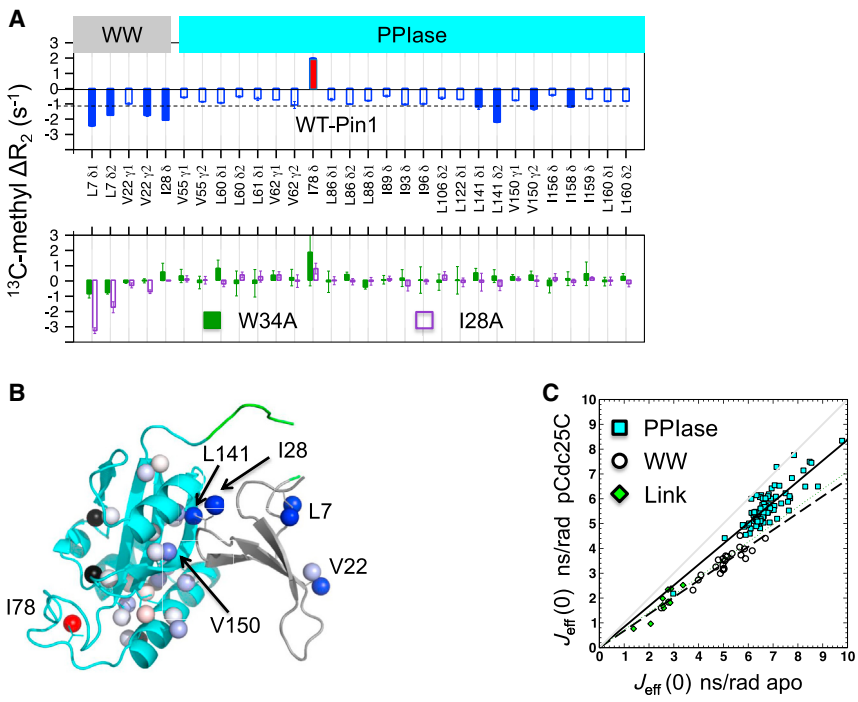

Figure 4. Changes in $^{13}C_{methyl}$ and ^{15}N Relaxation Parameters due to pCdc25C Binding

(A) Differences $\Delta R_2 = R_{2,pCDC25} - R_{2,APO}$ for $^{13}C_{methyl}HD_2$ groups. $R_{2,pCDC25}$ values correspond to a 7-fold molar excess of pCdc25C over protein. Upper: WT-Pin1, where filled blue bars highlight sites of large-magnitude changes beyond the trimmed average $<\Delta R_2> = -0.9\ s^{-1}$ (dashed horizontal line). Lower: W34A (solid green) and I28A (open violet). R_2 experiments used CPMG spin locks with interpulse delays of 900 μs. Fractional uncertainties in R_2 values were estimated using Monte Carlo simulations of duplicate spectra, in the range 1%–2%.

(B) $R_{2,pCDC25} - R_{2,APO}$ mapped onto 1PIN1 ILV methyls (shaded spheres). Sphere shading indicates ΔR_2 values via a continuous gradient from blue (large decrease) to white (no change) to red (large increase) upon pCdc25C binding. Black spheres are methyls whose resonances are overlapped and omitted from analysis. The lone red sphere is I78δ.

(C) Linear correlation of backbone NH $J_{eff}(0)$ for apo WT-Pin1 (horizontal axis) versus $J_{eff}(0)$ for pCdc25C/WT-Pin1 (7:1) (vertical axis). The symbols indicate NH bonds of the WW domain (open circles), PPIase domain (cyan squares), and flexible linker (green diamonds). Linear regression: WW domain: slope = 0.68, correlation coefficient = 0.94; PPIase domain: slope = 0.84, correlation coefficient = 0.90.

which enhances peptidyl-prolyl isomerase activity at the remote PPIase catalytic pocket. We therefore propose that interdomain contact within Pin1 can provide negative allosteric regulation of the PPIase catalytic site. Here, we discuss a model for this regulation that builds on our previous evidence for intradomain allostery, indicated by the orange arrows in Figure 5A. We first highlight the intradomain allostery, and then how they cooperate for interdomain allostery.

Intradomain Allosteric Communication

In the WW domain, the communication is between loops 1 and 2, which interact with pCdc25C and the PPIase domain, respectively. Loop 2 does not contact substrate. Nevertheless, the I28A substitution in loop 2 reduced interdomain contact and weakened pCd25C binding affinity by ~5-fold, suggesting intradomain allostery (Wilson et al., 2013). A plausible mechanism for loop 1-loop 2 allosteric communication are long-range correlated motions, which emerged in our previous molecular dynamics simulations of the isolated WW domain (Morcos et al., 2010).

In the PPIase domain, several pieces of evidence indicate intradomain allosteric communication between the catalytic pocket and the distal interdomain interface (α4/β6 region). First, a *cis*-locked inhibitor that bound only to the PPIase catalytic pocket demonstrated higher binding affinity for the isolated PPIase domain compared with full-length Pin1 (Namanja et al., 2011). Second, the isolated PPIase domain showed slightly higher isomerase activity (k_{EXSY}) toward pCdc25C than full-length Pin1 (Namanja et al., 2011), a trend observed with other phosphopeptide substrates (Greenwood et al., 2011). Third, the changes in subnanosecond flexibility for methyl-bearing side chains caused by pCdc25C binding included losses along a conduit of conserved hydrophobic residues (Figure 5B, right, red spheres) linking the PPIase interdomain interface (α4/β6) to the catalytic pocket (Namanja et al., 2007). These conduit residues, along with those showing strong pCdc25C-induced NH CSPs in the same general regions (Figure 5B, left, red shading), are the likely enablers of PPIase intradomain allostery.

Interdomain Allosteric Communication

The intradomain phenomena above lead to our model of interdomain allosteric communication in Figure 5C. Specifically, in apo WT-Pin1, the WW and PPIase domains engage in transient contacts between the α4/β6 region of the PPIase domain, P9, W11, I28-S32 (loop 2), and P37 in the WW domain (Bayer et al., 2003; Jacobs et al., 2003). In the simplest case, the contact transience reflects Pin1 exchanging between "open" and "closed" subensembles in equilibrium as proposed by Bayer et al. (2003). The actual apo conformational ensemble may be more complex, but within the ensemble the domains will still sample a range of dispositions, some more intimate than others.

A critical stipulation is that the catalytic pocket of the apo PPIase domain in full-length Pin1 samples local conformations sufficiently distinct from those of isolated PPIase domain, to yield different isomerization activities ($k_{EXSY,WT\text{-}PPIase} > k_{EXSY,WT\text{-}Pin1}$, Table 1). The cartoons in Figure 5C depict this with the oval-shaped catalytic pocket in Pin1 versus the optimal "matched" trapezoidal pocket in the isolated PPIase domain.

When pCdc25C is introduced, it binds preferentially to the Pin1 WW domain via W34 and loop 1, thereby perturbing loop 2 at the domain interface (residues H27–N30) via the intradomain WW allostery described above. This triggers a loss of interdomain contact. In effect, pCdc25C binding stabilizes a subset of WW conformations favoring reduced interdomain contact, as

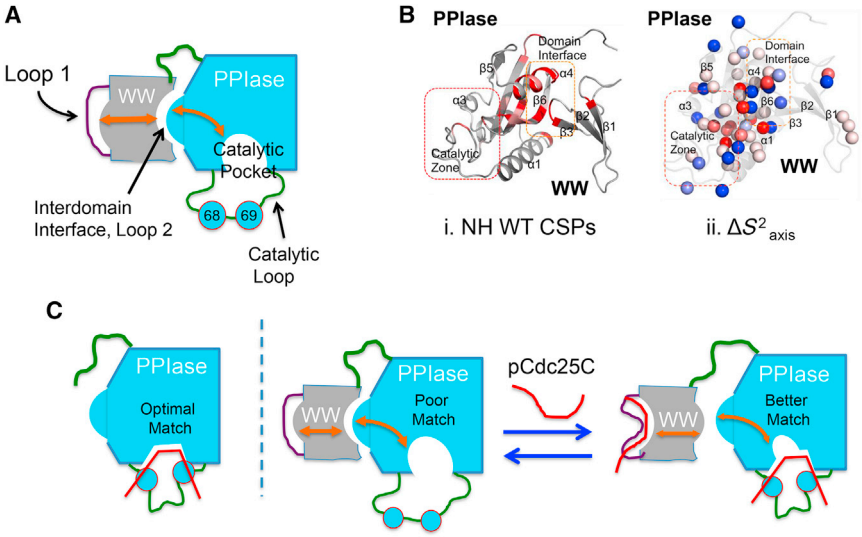

Figure 5. Schematic of Allosteric Communication in Pin1

(A) Intradomain allosteric coupling (orange arrows). WW domain coupling is between the substrate-binding loop 1 (S16-R21) and interdomain interface loop 1 (H27-N30). PPIase domain coupling is between the interdomain interface and the catalytic active site.

(B) Residues believed to enable allostery within the PPIase domain, based on NH CSPs and changes in methyl side-chain flexibility, ΔS^2_{axis} due to pCdc25C binding from previous work (Namanja et al., 2007): Red shading of the left structure shows NH CSPs >0.02 ppm for the PPIase domain and interdomain interface. The right structure has methyl carbons (spheres) colored according to ΔS^2_{axis}, where blue indicates gain of flexibility, white no change, and red loss of flexibility, $\Delta S^2_{axis} > 0$. Red spheres trace the conduit of flexibility loss due to pCdc25C binding.

(C) Model for allosteric regulation of interdomain contact on PPIase activity. The catalytic pocket of the isolated PPIase domain is optimally matched for *cis-trans* isomerization. In full-length apo Pin1, interdomain contact promotes catalytic pocket conformations that are suboptimal for isomerization. Binding of pCdc25C at WW domain loop 1 weakens interdomain interactions, allosterically altering the catalytic pocket conformations relevant for isomerization.

evidenced by the α4/β6 CSPs resembling deletion of the WW domain (e.g. Figures 2 and 3). The cartoon in Figure 5C models this via decreased surface complementarity between the domains.

The loss of interdomain contact perturbs the local packing of side-chain contacts that link the interdomain interface to the catalytic pocket. This manifests as the α4/β6 CSP surge in the PPIase domain, and the dynamic conduit observed in our first Pin1 studies (Namanja et al., 2007). The net effect alters the local conformations sampled by catalytic pocket to those resembling the isolated PPIase domain (Figure 5C, far right). *cis-trans* isomerization proceeds with the WT rate constant, $k_{EXSY,WT\text{-}Pin1}$. Because the conformational ensemble of the catalytic pocket resembles rather than matches that of the isolated PPIase domain, we observe $k_{EXSY,WT\text{-}Pin1} < k_{EXSY,WT\text{-}PPIase}$ (Table 1).

Interdomain Contact and Negative Allosteric Regulation

The aforestated model proposes that interdomain contact provides allosteric regulation, and derives heavily from the contrast between WT-Pin1 and W34A-Pin1, two proteins with different isomerase activities and interdomain interfaces. Upon pCdc25C binding to its WW domain, WT-Pin1 loses interdomain contact. By contrast, W34A-Pin1 has comparatively negligible binding of pCdc25C, and so sustains its apo level of interdomain contact, as shown in Figures 3A and 3B. In effect, W34A-Pin1 reveals the isomerase activity that would prevail, *if* the apo state interdomain contact were sustained. With no change in interdomain contact, the W34A-Pin1 PPIase catalytic pocket retains its suboptimal configuration, producing the lower pCdc25C *cis-trans* rate constants compared with WT-Pin1 (i.e. $k_{EXSY,W34A} < k_{EXSY,WT\text{-}Pin1}$, Table 1). The effects of W34A-Pin1 and the other mutants are schematized in Figure S5.

I28A reduces interdomain contact in the apo state (Wilson et al., 2013), likely because the substitution incurs the loss of the branched hydrophobic side chain promoting interdomain contact. Adding pCdc25C elicits no further reduction, as shown by the NH CSPs (Figure 3A) and A140 and L141 cross-peak positions (Figure 3B). Thus, before pCdc25C binds, I28A PPIase domain is already in a configuration yielding higher k_{EXSY}. We therefore expect and observe greater *cis-trans* isomerase activity for I28A-Pin1 than for WT-Pin1 ($k_{EXSY,I28A} > k_{EXSY,WT\text{-}Pin1}$, Table 1). I28A-Pin1 also has greater *cis-trans* isomerase activity than the isolated PPIase domain ($k_{EXSY,I28A} > k_{EXSY,PPIase}$, Table 1). This inequity may reflect the local enhancement of substrate concentration via the WW domain that I28A-Pin1 can enjoy but the isolated PPIase domain cannot.

For R68A/R69A-Pin1, the alanine substitutions break contacts between the catalytic loop and the substrate pS/T motif, quashing isomerase activity (Table 1). By contrast, the interdomain interface and WW domain are unperturbed (Figure 2A, panel i), and so the pCdc25C K_D is almost the same as that of WT-Pin1. We therefore expect the observed α4/β6 CSP surge, diagnostic of reduced interdomain contact (Figure 3, panel ii).

The exchange rate constant is the sum $k_{EXSY} = k_{TC} + k_{CT}$, where k_{TC} and k_{CT} indicate *trans*-to-*cis* and *cis*-to-*trans*, respectively. Table 1 also shows that the WW substitutions generally altered k_{TC} (*trans*-to-*cis*) rather than k_{CT} (*cis*-to-*trans*). While the underlying reasons for this are unclear, we speculate that it reflects perturbations of the Michaelis constant, $K_{M,trans}$, for *trans* pCdc25C substrate binding to the PPIase catalytic pocket. The $K_{M,trans}$ value is sensitive to at least two factors: appropriate conformational sampling of the catalytic pocket to bind *trans* substrate, and the availability of *trans* substrate itself. Both factors can change upon mutation or deletion of the WW domain, which preferentially binds the *trans* substrate (as in the case of pCdc25C) (Lippens et al., 2007), leading to reduced interdomain contact.

Implications for Subnanosecond Side-Chain Flexibility

Our first NMR study of Pin1 functional motions explored side-chain flexibility, focusing on subnanosecond reorientational

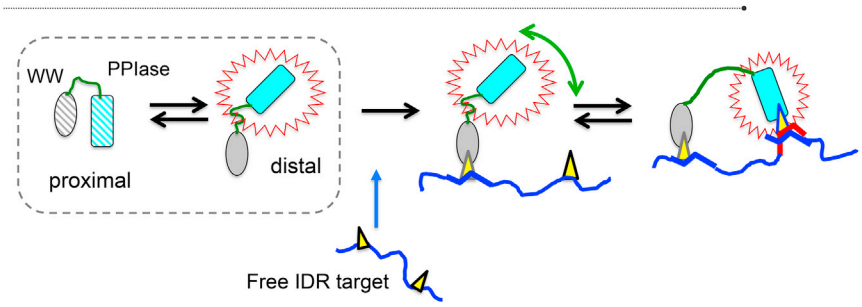

Figure 6. Speculative Model for Pin1 Interaction with Multiple pS/T-P Sites
WW domain recognition of one pS/T-P motif reduces interdomain contact, which then tunes the PPIase domain catalytic site for binding another pS/T-P motif. The observed negative regulation of the PPIase domain via interdomain contact stems from parallel recognition by the two domains that resembles "fly-casting" (Shoemaker et al., 2000).

motions of methyl-bearing side chains (Namanja et al., 2007). That study included backbone ^{15}N relaxation measurements to estimate domain-specific correlation times for overall tumbling. Our results echoed those of the earlier investigation by Jacobs et al. (2003); namely, pCdc25C binding increased the independence of domain tumbling, implying decreased interdomain contact. Yet the side chains suggested a more complex response for the very same binding event. In particular, we mapped the changes in the amplitudes of internal motion for the methyl symmetry axes via order parameters S^2_{axis}, and their changes upon binding pCdc25C, $\Delta S^2_{axis} = S^2_{axis,pCdc25C} - S^2_{axis,APO}$ (Namanja et al., 2007). As is common for side chains (Igumenova et al., 2006), both positive and negative ΔS^2_{axis} emerged, corresponding to both losses and gains in side-chain flexibility (Namanja et al., 2007). The flexibility losses defined a "conduit" of highly conserved hydrophobic residues connecting the interdomain interface to the catalytic site (Figure 5B, right structure, red spheres). It has been shown that S^2_{axis} values are sensitive to local packing and the density of steric (van der Waals) contacts (Buck et al., 1995; Ming and Brüschweiler, 2004). Hence, increased S^2_{axis} upon pCdc25C binding indicated local compaction, and thus raised the possibility of an *increase* in Pin1 interdomain contact. Resolving the backbone versus side chain pictures for this particular pCdc25C substrate remained an open issue for us.

Our mutation studies herein provide strong evidence supporting the reduction of Pin1 interdomain contact by pCdc25C binding; hence, its conduit response must reflect this reduction. This "reduced contact" interpretation is consistent with our more recent studies of Pin1 interacting with other substrates. For example, Figure 5C would predict that substrates having different effects on interdomain contact would yield different patterns of S^2_{axis} change. This prediction is borne out by Pin1's interaction with a wholly different substrate sequence, FFpSPR, which does *not* reduce interdomain contact (Namanja et al., 2011). In particular, plots of $J_{eff}(0)$ for apo WT-Pin1 (horizontal axis) versus $J_{eff}(0)$ for FFpSPR-saturated WT-Pin1 (vertical axis) show essentially the same slope for the WW and PPIase domains (WW slope = 0.85, correlation coefficient of 0.94; PPIase slope = 0.87, correlation coefficient of 0.8), indicating no loss of interdomain contact. The changes in side-chain flexibility caused by FFpSPR reveal a conduit similar to that of pCdc25C, but which also displays significant local differences within the catalytic pocket (Namanja et al., 2011). These comparisons are shown in Figure S6.

We can speculate as to how reduced interdomain contact could reduce side-chain flexibility at the interdomain interface, and within the PPIase hydrophobic core. In full-length apo Pin1, the PPIase $\alpha4/\beta6$ region may sample multiple, roughly isoenergetic conformations that favor either intradomain contact or interdomain contact with the WW domain. This manifests as conformational flexibility on potentially multiple timescales. The availability of interdomain contacts vanishes when pCdc25C binds the WW domain, or deletion of the WW domain. As a result, the breadth of accessible $\alpha4/\beta6$ conformations shrinks, which manifests as local decreases in flexibility (the conduit response). To go beyond speculation, we have begun explicit-solvent molecular dynamics simulations for WT-Pin1 and the mutants, with the goal of generating sufficiently long trajectories to enable cross-validation against the NMR data, and direct comparisons of side-chain order parameters S^2_{axis} from molecular dynamics versus NMR (Kasinath et al., 2013; Showalter and Brüschweiler, 2007).

Significance

Reduced interdomain Pin1 contact upon pCdc25C binding had been suggested previously (Jacobs et al., 2003), but its underlying mechanism and functional implications have remained unclear. Our studies herein begin to provide some clarity, by exposing the residues regulating interdomain contact and showing that reduced contact can enhance PPIase activity. These findings indicate that Pin1 interdomain contact can provide negative allosteric regulation of its isomerase activity.

Negative allosteric regulation has implications for how Pin1 interacts with its protein substrates, which often have multiple pS/T-P motifs within IDRs. An example is Cdc25C phosphatase, which has up to five pS/T-P motifs in its disordered N-terminal regulatory domain (Kumagai and Dunphy, 1997; Stukenberg and Kirschner, 2001). The multiplicity of pS/T-P sites within flexible regions allows for a diversity of substrate conformations, with an attendant need for multiple interaction mechanisms by Pin1.

Our work here suggests that some of these mechanisms may involve parallel recognition, as depicted in Figure 6. In this speculative model, WW domain binds a *trans* pS/T-P motif first, due to its higher substrate-binding affinity relative to the PPIase domain (Verdecia et al., 2000). WW domain binding of the first motif weakens the apo state interdomain contact, thus freeing the PPIase domain to search for a distinct pS/T-P site, with a catalytic site more adept for *cis-trans* isomerization. Localization of the PPIase domain to the IDR region via the bound WW domain would increase the local concentration of proximal pS/T-P sites, and help compensate for the intrinsically weaker substrate-binding affinity of the PPIase domain. Figure 6 resembles fly-casting, first proposed by Wolynes and co-workers (Shoemaker et al.,

2000). For this scheme to be tenable, Pin1 must be capable of dual ligand occupancy. Indeed, our previous work with conformationally locked inhibitors showed that Pin1 has this capability (Namanja et al., 2011); the WW and PPIase domains simultaneously bound distinct inhibitors: the *trans*-locked inhibitor in the WW domain, and the *cis*-locked inhibitor in the PPIase domain. Also, our NMR conditions typically involve a molar excess of pCdc25C over Pin1, and thus promote such dual occupancy.

We emphasize that different Pin1 phosphopeptide substrates can yield different perturbations to interdomain contact (Jacobs et al., 2003). We noted the example of FFpSPR. This substrate does not reduce interdomain contact (Namanja et al., 2011); it produces a conduit response similar to pCdc25C, but with local differences in the catalytic pocket (Figure S6). Recent computational studies by Zhou and co-workers highlight the degrees of freedom for FFpSPR recognition (Guo et al., 2015). Our work here provides complementary insight into those Pin1 substrates that reduce interdomain contact, such as pCdc25C.

In conclusion, we provide evidence for negative allosteric regulation of the PPIase domain activity of Pin1 by interdomain contact with the WW domain. Such regulation would be compatible with Pin1 recognition of multiple pS/T-P sites in IDRs. The advantage of IDRs is likely more rapid access to pS/T-P sites by kinases and phosphatases. An IDR environment suggests the existence of diverse Pin1-mediated responses, with different cohorts of pS/T-P motifs sampling different local conformations that select for different interdomain configurations on the part of Pin1. If so, the design of ligands that stabilize distinct Pin1 interdomain configurations may promote specific inhibition of Pin1/substrate interactions.

EXPERIMENTAL PROCEDURES

Sample Preparation

The expression and purification procedures of Pin1 and isolated PPIase constructs followed procedures described in our previous work (Namanja et al., 2011). New Pin1 mutants in this work were constructed using a megaprimer PCR strategy (Sarkar and Sommer, 1990) (primers used are listed in in Table S1). The genes were inserted into the pET41b vector (Novagen), clones selected, and their DNA sequences verified. ILV labeling (i.e. U-^{15}N-, Ileδ_1-[$^{13}CHD_2$]-, Leuδ_1/δ_2[$^{13}CHD_2]_2$-, and Valγ_1/γ_2-[$^{13}CHD_2]_2$-), produced $^{13}CHD_2$ methyl groups for I, L, and V. Expression of ILV-Pin1 and Pin1 variants followed published protocols (Tugarinov et al., 2006; Tugarinov and Kay, 2004). SDS-PAGE analysis verified greater than 98% purity for all proteins. Samples were exchanged into Pin1 NMR buffer (30 mM imidazole-d4 [CIL] [pH 6.6], 30 mM NaCl, 0.03% NaN_3, 5 mM DTT-d10, and 90% H_2O/10% D_2O). ^{15}N-^{1}H HSQCs confirmed proper folding of constructs (Figure S1). The phosphopeptide substrate EQPLpTPVTDL (pCdc25C) was purchased from Anaspec.

NMR Spectroscopy and Analysis

NMR spectra were recorded at 295 K on Bruker Avance 700 MHz (16.4T) and 800 MHz (18.8 T) spectrometers with TCI cryogenic probes. Time-domain data were processed using Topspin 1.3 and 2.1 (Bruker Biospin), and spectra were assigned using Sparky (SPARKY 3; T.D. Goddard and D.G. Kneller, University of California San Francisco).

The ^{15}N-^{1}H CSPs were evaluated from fast-HSQC (Mori et al., 1995) and transverse relaxation optimized spectroscopy-HSQC (Pervushin et al., 1997; Rance et al., 1999) spectra (^{15}N sweep width of 35.24 ppm, 75 complex points), for non-deuterated and deuterated Pin1, respectively. The ^{15}N-^{1}H CSPs between two protein conditions, A and B, were

$$\Delta\delta_{NH} = \sqrt{(\delta H_A - \delta H_B)^2 + (0.154\ (\delta N_A - \delta N_B))^2}. \quad \text{(Equation 1)}$$

For evaluating basic mutation effects as in Figure 2, conditions A and B were the apo WT and apo mutants. For binding studies (Figure 3), A and B were protein in the absence and presence of ligand, respectively. The binding-related CSPs were interpreted in terms of the equilibrium

$$PL \rightleftarrows P + L, \quad \text{(Equation 2)}$$

where P, L, and PL represented free protein, free ligand, and protein-ligand complex, respectively. We fitted the CSPs versus the ratio of total ligand to total protein (L_T/P_T) to

$$\Delta\delta_{NH} = \frac{\Delta\delta_{NH,MAX}}{2}\left\{\left(1 + \frac{L_T}{P_T} + \frac{K_D}{P_T}\right) - \sqrt{\left(1 + \frac{L_T}{P_T} + \frac{K_D}{P_T}\right)^2 - \frac{4L_T}{P_T}}\right\}, \quad \text{(Equation 3)}$$

which assumes the binding exchange is fast on the chemical shift timescale. The global dissociation constant, K_D, and specific parameters, $\Delta\delta_{NH,MAX}$, were determined by using standard non-linear least-squares methods and jack-knife simulations for error estimates (Press et al., 1992). K_D was stepped in a one-dimensional grid search. For a fixed K_D value, the individual $\Delta\delta_{NH,MAX}$, were optimized using non-linear least squares. The process was repeated until convergence.

Pin1 *cis-trans* activity toward pCdc25C was measured at 295 K and 16.4 T, by following *cis-trans* exchange of longitudinal magnetization of pT5-^{1}Hγ methyl nuclei via 2D ^{1}H-^{1}H exchange spectroscopy (EXSY) spectra (Jeener et al., 1979). Samples consisted of 50 μM fresh protein (WT-Pin1, W34A-Pin1, R68A-Pin1, I28A-Pin1) in the presence of 2 mM Cdc25C phosphopeptide substrate. Exchange mixing times were 6.1, 11.1, 51.1 (×2), 76.1, 101.1, 151.1, 201.1, 226.1, 301.1, 351.1, and 451.1 (×2) ms. EXSY spectra of 2 mM isolated pCdc25C under the same conditions gave no exchange cross-peaks, indicating that the thermal *cis-trans* isomerization was too slow for detection. Exchange rate constants, k_{EXSY}, were estimated by fitting the ratios of *trans*-to-*cis* exchange cross-peaks over the *trans* diagonal peaks as a function of the exchange mixing time to the two-state function (Ernst et al., 1987).

$^{13}C_{methyl}$ and ^{15}N relaxation measurements were at 295 K and 16.4 T. $^{13}C_{methyl}$ R_2 measurements on ILV samples used standard 2D ^{1}H-detected in-phase $^{13}C_{methyl}$ R_2 measurements for AX spin systems (Nirmala and Wagner, 1988; Palmer et al., 1991), and CPMG (Carr and Purcell, 1954; Meiboom and Gill, 1958) relaxation dispersion (Blackledge et al., 1993; Deverell et al., 1970) with compensation for ^{13}C-^{1}H scalar coupling (Loria et al., 1999; Skrynnikov et al., 2001). The ^{13}C dimension of the 2D $^{13}C_{methyl}$-^{1}H relaxation spectra included a ^{13}C sweep width of 20.14 ppm and 64 complex points, with the ^{13}C carrier at 15.5 ppm. ^{13}C CPMG spin locking involved 75-μs refocusing pulses; the interpulse delay, t_{cp}, was fixed at 900 μs for $^{13}C_{methyl}$ R_2 measurements, and varied as $t_{cp} = 1/2\nu_{CPMG}$ for dispersion. Long t_{cp} values (>3 ms) included deuterium 180° decoupling pulses to suppress relaxation artifacts from ^{13}C-^{2}D scalar coupling (~22 Hz). $^{13}C_{methyl}$ R_2 relaxation delays included T = 7.8, 15.6, 23.4, 31.2, 39.0, 46.8, 54.6, 62.4, 70.2, 78.0, and 85.8 ms. The ν_{CPMG} values for WT-Pin1 were 31, 62, 94, 125, 158, 190, 223, 256, 289, 323, 357, 391, 426, 461, and 496 Hz; for I28A-Pin1 and W34A-Pin1, the ν_{CPMG} values were 94, 125, 148, 190, 289, 391, 496, 532, 604, 640, and 715 Hz. Dispersion reference spectra (CPMG absent) were collected twice. $^{13}C_{methyl}$ R_1 values for ILV-labeled WT-Pin1 were measured by using a $^{13}C_{methyl}$ adapted version of the standard ^{15}N R_1 scheme (Chen and Tjandra, 2011). The R_1 relaxation delays included 42, 98 (×2), 196, 393, 491.5, 786, 997, and 1,994 ms. Otherwise, the 2D spectral parameters were the same as in $^{13}C_{methyl}$ R_2.

$^{13}C_{methyl}$ R_1 and R_2 were determined by standard non-linear least-squares fitting of cross-peak volumes $I(T)$ versus relaxation delay T to $I(T) = I_0 \exp(-R_{1,2}T)$, followed by Carlo analysis for error estimates (Press et al., 1992). $^{13}C_{methyl}$ $R_{2,eff}$ values from dispersion spectra were determined from $R_{2,eff}(1/2t_{cp}) = 1/T \cdot \ln\{I(1/2t_{cp})/I_{ref}\}$ (Mulder et al., 2001), where $I(1/2t_{cp})$ and I_{ref} were cross-peak volumes with the CPMG present and absent. Jack-knife simulations provided error estimates.

Backbone ^{15}N R_1, R_2, and ^{1}H-^{15}N ssNOE measurements at 16.4 T used standard ^{1}H-detected 2D methods described previously (Namanja et al., 2007). The same relaxation delays were used for apo and complexed samples.

$R_1(^{15}N)$ delays included T = 106.6 (×2), 213.2, 426.4, 639.6, 852.8, 1,066, 1,279.2, and 1,492.4 ms. ^{15}N R_2 measurements used CPMG spin locking with 100-μs refocusing pulses and interpulse delay of 900 μs. R_2 delays were T = 16 (×2), 24, 32, 40, 48, 56, 72, and 88 ms. ^1H-^{15}N ssNOEs were measured in an interleaved manner to give spectra corresponding to the absence and presence of 5s ^1H saturation (two spectra each). The ^{15}N R_1, R_2, and ssNOE values were determined from 2D cross-peak volumes using standard fitting procedures described previously (Wilson et al., 2013).

For each NH bond, we determined reduced spectral densities, $J_{eff}(0)$, $J(\omega_N)$, and $<J(\omega_H)>$ (Farrow et al., 1995; Ishima and Nagayama, 1995; Peng and Wagner, 1995) using the following relationships (Peng and Wagner, 1995):

$$J_{eff}(0) = \frac{3}{2(3D+C)}\left(R_2 - \frac{R_1}{2} - \frac{3\sigma_{NH}}{5}\right)$$
$$J(\omega_N) = \frac{1}{(3D+C)}\left(R_1 - \frac{7\sigma_{NH}}{5}\right) \quad \text{(Equation 4)}$$
$$\langle J(\omega_H)\rangle = \frac{\sigma_{NH}}{5D}$$

where σ_{NH} was extracted from

$$ssNOE = \left(\frac{N_{z,saturation} - N_{z,eq}}{N_{z,eq}}\right) = \frac{\gamma_H}{\gamma_N}\frac{\sigma_{NH}}{R_1(N)}. \quad \text{(Equation 5)}$$

The C and D constants in Equation 4 pertain to the ^{15}N chemical shift anisotropy and ^{15}N-^1H dipolar relaxation mechanisms, respectively: $C = \Delta^2\omega_N^2/3$ and $D = \hbar^2\gamma_H^2\gamma_N^2/4\langle r_{HN}^6\rangle$.

SUPPLEMENTAL INFORMATION

Supplemental Information includes six figures and one table and can be found with this article online at http://dx.doi.org/10.1016/j.str.2015.08.019.

ACKNOWLEDGMENTS

We are grateful to Dr. Ad Bax, Dr. Jill J. Bouchard, Dr. Kimberly A. Wilson, Mr. Thomas Frederick, and Mr. Michael Staude for valuable suggestions and discussions. This work was supported by NIH Grant R01-GM083081 (J.W.P.).

Received: December 13, 2014
Revised: August 22, 2015
Accepted: August 24, 2015
Published: October 22, 2015

REFERENCES

Bayer, E., Goettsch, S., Mueller, J.W., Griewel, B., Guiberman, E., Mayr, L.M., and Bayer, P. (2003). Structural analysis of the mitotic regulator hPin1 in solution: insights into domain architecture and substrate binding. J. Biol. Chem. *278*, 26183–26193.

Blackledge, M.J., Brüschweiler, R., Griesinger, C., Schmidt, J.M., Xu, P., and Ernst, R.R. (1993). Conformational backbone dynamics of the cyclic decapeptide antamanide. Application of a new multiconformational search algorithm based on NMR data. Biochemistry *32*, 10960–10974.

Buck, M., Boyd, J., Redfield, C., MacKenzie, D.A., Jeenes, D.J., Archer, D.B., and Dobson, C.M. (1995). Structural determinants of protein dynamics: analysis of 15N NMR relaxation measurements for main-chain and side-chain nuclei of hen egg white lysozyme. Biochemistry *34*, 4041–4055.

Carr, H.Y., and Purcell, E.M. (1954). Effects of diffusion on free precession in nuclear magnetic resonance experiments. Phys. Rev. *94*, 630–638.

Chen, C.H., Chang, C.C., Lee, T.H., Luo, M., Huang, P., Liao, P.H., Wei, S., Li, F.A., Chen, R.H., Zhou, X.Z., et al. (2013). SENP1 deSUMOylates and regulates Pin1 protein activity and cellular function. Cancer Res. *73*, 3951–3962.

Chen, K., and Tjandra, N. (2011). Water proton spin saturation affects measured protein backbone ^{15}N spin relaxation rates. J. Magn. Reson. *213*, 151–157.

Crenshaw, D.G., Yang, J., Means, A.R., and Kornbluth, S. (1998). The mitotic peptidyl-prolyl isomerase, Pin1, interacts with Cdc25 and Plx1. EMBO J. *17*, 1315–1327.

Deverell, C., Morgan, R.E., and Strange, J.H. (1970). Studies of chemical exchange by nuclear magnetic relaxation in the rotating frame. Mol. Phys. *18*, 553.

Ernst, R.R., Bodenhausen, G., and Wokaun, A. (1987). Dynamic processes studied by two-dimensional exchange spectroscopy. In Principles of Nuclear Magnetic Resonance in One and Two Dimensions (Oxford Science Publications), p. 498.

Farrow, N.A., Zhang, O., Szabo, A., Torchia, D.A., and Kay, L.E. (1995). Spectral density function mapping using ^{15}N relaxation data exclusively. J. Biomol. NMR *6*, 153–162.

Greenwood, A.I., Rogals, M.J., De, S., Lu, K.P., Kovrigin, E.L., and Nicholson, L.K. (2011). Complete determination of the Pin1 catalytic domain thermodynamic cycle by NMR lineshape analysis. J. Biomol. NMR *51*, 21–34.

Guo, J., Pang, X., and Zhou, H.X. (2015). Two pathways mediate interdomain allosteric regulation in pin1. Structure *23*, 237–247.

Igumenova, T.I., Frederick, K.K., and Wand, A.J. (2006). Characterization of the fast dynamics of protein amino acid side chains using NMR relaxation in solution. Chem. Rev. *106*, 1672–1699.

Ishima, R., and Nagayama, K. (1995). Protein backbone dynamics revealed by quasi spectral density function analysis of amide N-15 nuclei. Biochemistry *34*, 3162–3171.

Jacobs, D.M., Saxena, K., Vogtherr, M., Bernado, P., Pons, M., and Fiebig, K.M. (2003). Peptide binding induces large scale changes in inter-domain mobility in human Pin1. J. Biol. Chem. *278*, 26174–26182.

Jeener, J., Meier, B.H., Bachmann, P., and Ernst, R.R. (1979). Investigation of exchange processes by two-dimensional NMR spectroscopy. J. Chem. Phys. *71*, 4546–4553.

Kasinath, V., Sharp, K.A., and Wand, A.J. (2013). Microscopic insights into the NMR relaxation-based protein conformational entropy meter. J. Am. Chem. Soc. *135*, 15092–15100.

Kneller, J.M., Lu, M., and Bracken, C. (2002). An effective method for the discrimination of motional anisotropy and chemical exchange. J. Am. Chem. Soc. *124*, 1852–1853.

Kumagai, A., and Dunphy, W.G. (1997). Regulation of *Xenopus* Cdc25 protein. Methods Enzymol. *283*, 564–571.

Lee, T.H., Chen, C.H., Suizu, F., Huang, P., Schiene-Fischer, C., Daum, S., Zhang, Y.J., Goate, A., Chen, R.H., Zhou, X.Z., et al. (2011). Death-associated protein kinase 1 phosphorylates Pin1 and inhibits its prolyl isomerase activity and cellular function. Mol. Cell *42*, 147–159.

Lee, C., Kalmar, L., Xue, B., Tompa, P., Daughdrill, G.W., Uversky, V.N., and Han, K.H. (2014). Contribution of proline to the pre-structuring tendency of transient helical secondary structure elements in intrinsically disordered proteins. Biochim. Biophys. Acta *1840*, 993–1003.

Lippens, G., Landrieu, I., and Smet, C. (2007). Molecular mechanisms of the phospho-dependent prolyl cis/trans isomerase Pin1. FEBS J. *274*, 5211–5222.

Loria, J.P., Rance, M., and Palmer, A.G., 3rd (1999). A relaxation-compensated Carr-Purcell-Meiboom-Gill sequence for characterizing chemical exchange by NMR spectroscopy. J. Am. Chem. Soc. *121*, 2331–2332.

Lu, K.P., and Zhou, X.Z. (2007). The prolyl isomerase PIN1: a pivotal new twist in phosphorylation signalling and disease. Nat. Rev. Mol. Cell Biol. *8*, 904–916.

Lu, K.P., Hanes, S.D., and Hunter, T. (1996). A human peptidyl-prolyl isomerase essential for regulation of mitosis. Nature *380*, 544–547.

Lu, P.J., Wulf, G., Zhou, X.Z., Davies, P., and Lu, K.P. (1999). The prolyl isomerase Pin1 restores the function of Alzheimer-associated phosphorylated tau protein. Nature *399*, 784–788.

Lu, P.J., Zhou, X.Z., Liou, Y.C., Noel, J.P., and Lu, K.P. (2002). Critical role of WW domain phosphorylation in regulating phosphoserine binding activity and Pin1 function. J. Biol. Chem. *277*, 2381–2384.

Meiboom, S., and Gill, D. (1958). Modified spin-echo method for measuring nuclear relaxation times. Rev. Sci. Instrum. *29*, 688–691.

Ming, D., and Brüschweiler, R. (2004). Prediction of methyl-side chain dynamics in proteins. J. Biomol. NMR *29*, 363–368.

Morcos, F., Chatterjee, S., McClendon, C.L., Brenner, P.R., Lopez-Rendon, R., Zintsmaster, J., Ercsey-Ravasz, M., Sweet, C.R., Jacobson, M.P., Peng, J.W., et al. (2010). Modeling conformational ensembles of slow functional motions in Pin1-WW. PLoS Comput. Biol. *6*, e1001015.

Mori, S., Abeygunawardana, C., Johnson, M.O., and van Zijl, P.C. (1995). Improved sensitivity of HSQC spectra of exchanging protons at short interscan delays using a new fast HSQC (FHSQC) detection scheme that avoids water saturation. J. Magn. Reson. B *108*, 94–98.

Mulder, F.A.A., de Graaf, R.A., Kaptein, R., and Boelens, R. (1998). An off-resonance rotating frame relaxation experiment for the investigation of macromolecular dynamics using adiabatic rotations. J. Magn. Reson. *131*, 351–357.

Mulder, F.A., Mittermaier, A., Hon, B., Dahlquist, F.W., and Kay, L.E. (2001). Studying excited states of proteins by NMR spectroscopy. Nat. Struct. Biol. *8*, 932–935.

Namanja, A.T., Peng, T., Zintsmaster, J.S., Elson, A.C., Shakour, M.G., and Peng, J.W. (2007). Substrate recognition reduces side-chain flexibility for conserved hydrophobic residues in human Pin1. Structure *15*, 313–327.

Namanja, A.T., Wang, X.J., Xu, B., Mercedes-Camacho, A.Y., Wilson, K.A., Etzkorn, F.A., and Peng, J.W. (2011). Stereospecific gating of functional motions in Pin1. Proc. Natl. Acad. Sci. USA *108*, 12289–12294.

Nirmala, N.R., and Wagner, G. (1988). Measurement of ^{13}C relaxation times in proteins by two-dimensional heteronuclear ^{1}H-^{13}C correlation spectroscopy. J. Am. Chem. Soc. *110*, 7557–7558.

Palmer, A.G., 3rd, Rance, M., and Wright, P.E. (1991). Intramolecular motions of a zinc Finger DNA-binding domain from Xfin characterized by proton-detected natural abundance ^{13}C heteronuclear NMR spectroscopy. J. Am. Chem. Soc. *113*, 4371–4380.

Pastorino, L., Sun, A., Lu, P.J., Zhou, X.Z., Balastik, M., Finn, G., Wulf, G., Lim, J., Li, S.H., Li, X., et al. (2006). The prolyl isomerase Pin1 regulates amyloid precursor protein processing and amyloid-beta production. Nature *440*, 528–534.

Peng, J.W., and Wagner, G. (1992). Mapping of spectral densities of NH bond motions in eglin C using heteronuclear relaxation experiments. Biochemistry *31*, 8571–8586.

Peng, J.W., and Wagner, G. (1995). Frequency spectrum of NH bonds in eglin c from spectral density mapping at multiple fields. Biochemistry *34*, 16733–16752.

Pervushin, K., Riek, R., Wider, G., and Wüthrich, K. (1997). Attenuated T2 relaxation by mutual cancellation of dipole-dipole coupling and chemical shift anisotropy indicates an avenue to NMR structures of very large biological macromolecules in solution. Proc. Natl. Acad. Sci. USA *94*, 12366–12371.

Poolman, T.M., Farrow, S.N., Matthews, L., Loudon, A.S., and Ray, D.W. (2013). Pin1 promotes GR transactivation by enhancing recruitment to target genes. Nucleic Acids Res. *41*, 8515–8525.

Press, W.H., Teukolsky, S.A., Vetterling, W.T., and Flannery, B.P. (1992). Numerical Recipes in C: The Art of Scientific Computing (Cambridge University Press).

Rance, M., Loria, J.P., and Palmer, A.G.R. (1999). Sensitivity improvement of transverse relaxation-optimized spectroscopy. J. Magn. Reson. *136*, 92–101.

Ranganathan, R., Lu, K.P., Hunter, T., and Noel, J.P. (1997). Structural and functional analysis of the mitotic rotamase Pin1 suggests substrate recognition is phosphorylation dependent. Cell *89*, 875–886.

Sami, F., Smet-Nocca, C., Khan, M., Landrieu, I., Lippens, G., and Brautigan, D.L. (2011). Molecular basis for an ancient partnership between prolyl isomerase Pin1 and phosphatase inhibitor-2. Biochemistry *50*, 6567–6578.

Sarkar, G., and Sommer, S.S. (1990). The "megaprimer" method of site-directed mutagenesis. Biotechniques *8*, 404–407.

Shoemaker, B.A., Portman, J.J., and Wolynes, P.G. (2000). Speeding molecular recognition by using the folding funnel: the fly-casting mechanism. Proc. Natl. Acad. Sci. USA *97*, 8868–8873.

Showalter, S.A., and Brüschweiler, R. (2007). Quantitative molecular ensemble interpretation of NMR dipolar couplings without restraints. J. Am. Chem. Soc. *129*, 4158–4159.

Skrynnikov, N.R., Mulder, F.A., Hon, B., Dahlquist, F.W., and Kay, L.E. (2001). Probing slow time scale dynamics at methyl-containing side chains in proteins by relaxation dispersion NMR measurements: application to methionine residues in a cavity mutant of T4 lysozyme. J. Am. Chem. Soc. *123*, 4556–4566.

Smet, C., Wieruszeski, J.M., Buée, L., Landrieu, I., and Lippens, G. (2005). Regulation of Pin1 peptidyl-prolyl cis/trans isomerase activity by its WW binding module on a multi-phosphorylated peptide of Tau protein. FEBS Lett. *579*, 4159–4164.

Stukenberg, P.T., and Kirschner, M.W. (2001). Pin1 acts catalytically to promote a conformational change in Cdc25. Mol. Cell *7*, 1071–1083.

Tugarinov, V., and Kay, L.E. (2004). An isotope labeling strategy for methyl TROSY spectroscopy. J. Biomol. NMR *28*, 165–172.

Tugarinov, V., Scheurer, C., Brüschweiler, R., and Kay, L.E. (2004). Estimates of methyl ^{13}C and ^{1}H CSA values (Deltasigma) in proteins from cross-correlated spin relaxation. J. Biomol. NMR *30*, 397–406.

Tugarinov, V., Kanelis, V., and Kay, L.E. (2006). Isotope labeling strategies for the study of high-molecular-weight proteins by solution NMR spectroscopy. Nat. Protoc. *1*, 749–754.

Verdecia, M.A., Bowman, M.E., Lu, K.P., Hunter, T., and Noel, J.P. (2000). Structural basis for phosphoserine-proline recognition by group IV WW domains. Nat. Struct. Biol. *7*, 639–643.

Wilson, K.A., Bouchard, J.J., and Peng, J.W. (2013). Interdomain interactions ort interdomain communication in human Pin1. Biochemistry *52*, 6968–6981.

Wintjens, R., Wieruszeski, J.-M., Drobecq, H., Rousselot-Pailley, P., Buée, L., Lippens, G., and Landrieu, I. (2001). ^{1}H NMR study on the binding of Pin1 Trp-Trp domain with phosphothreonine peptides. J. Biol. Chem. *276*, 25150–25156.

Wulf, G.M., Liou, Y.C., Ryo, A., Lee, S.W., and Lu, K.P. (2002). Role of Pin1 in the regulation of p53 stability and p21 transactivation, and cell cycle checkpoints in response to DNA damage. J. Biol. Chem. *277*, 47976–47979.

Yaffe, M.B., Schutkowski, M., Shen, M., Zhou, X.Z., Stukenberg, P.T., Rahfeld, J.U., Xu, J., Kuang, J., Kirschner, M.W., Fischer, G., et al. (1997). Sequence-specific and phosphorylation-dependent proline isomerization: a potential mitotic regulatory mechanism. Science *278*, 1957–1960.

Yeh, E., Cunningham, M., Arnold, H., Chasse, D., Monteith, T., Ivaldi, G., Hahn, W.C., Stukenberg, P.T., Shenolikar, S., Uchida, T., et al. (2004). A signalling pathway controlling c-Myc degradation that impacts oncogenic transformation of human cells. Nat. Cell Biol. *6*, 308–318.

Zhou, X.Z., Kops, O., Werner, A., Lu, P.J., Shen, M., Stoller, G., Küllertz, G., Stark, M., Fischer, G., and Lu, K.P. (2000). Pin1-dependent prolyl isomerization regulates dephosphorylation of Cdc25C and tau proteins. Mol. Cell *6*, 873–883.